Bull. of Atmos. Sci.& Technol. (2024) 5:14
https://doi.org/10.1007/s42865-024-00074-x

RESEARCH

Southern Hemisphere baroclinic activity in seasonal forecasts

Laura Trentini[1] · Sandro Calmanti[2] · Alessandro Dell'Aquila[2] · Sara Dal Gesso[1] · Marco Venturini[1] · Marcello Petitta[1,3]

Received: 30 January 2024 / Accepted: 19 July 2024

Abstract
Accurate prediction of mid-latitude baroclinic activity is extremely relevant for understanding global climate dynamics and improving long-term weather forecasts. However, current seasonal forecast models struggle to accurately represent the variability of baroclinic activity in the Southern Hemisphere, which may affect their reliability and usefulness. Baroclinic instability in the mid-latitudes is a significant component of the climate system, as it is associated with the meridional transport of a large amount of energy and momentum. Therefore, the ability of the models to correctly predict the properties of the atmospheric circulation in this latitudinal region is a very important requirement. The aim of this study is to estimate the energy of atmospheric phenomena typical of the mid-latitudes, such as baroclinic perturbations, and to understand how seasonal forecasts can be practically used to assess the energy transfer in the atmosphere. We compare the Southern Hemisphere mid-latitude winter variability of the seasonal forecasts of the ECMWF, DWD and Météo France forecasting systems with the ERA5 reanalysis. The analysis is performed by computing the Hayashi spectra of the 500-hPa geopotential height field. Both the reanalysis and the seasonal forecast show a series of peaks in the spectral region of eastward-travelling waves, which corresponds to the high frequency and high wavenumber domain. We quantify the amount of energy released from the atmosphere by calculating the Baroclinic Amplitude Index. The results suggest that seasonal forecasts may not accurately capture the variability of geopotential height power spectra in the Southern Hemisphere, which poses a challenge in correctly distributing the energy over spatial and temporal dimensions. This study will show that this problem is particularly pronounced for wavenumber 4 over a period of 8 days. This misrepresentation likely contributes to the uncertainties in precipitation forecasting, with discrepancies exacerbated by a suboptimal description of baroclinic instability and dynamical components in the models. Our findings highlight the need for an improved representation of baroclinic processes in seasonal forecast models, which could lead to substantial advancements in long-term weather prediction capabilities and in a more complete understanding of climate dynamics.

Keywords Baroclinic waves · Seasonal forecasts · Planetary waves · Hayashi spectra · Climate services

Extended author information available on the last page of the article

Published online: 20 September 2024

1 Introduction

Meteorological forecasts are widely used for prediction up to 10 days. However, the need to extend the forecast range is becoming increasingly urgent, and in the last decade the major meteorological agencies have made efforts to produce forecasts on a seasonal scale. Unlike traditional deterministic forecasts, which are limited by the predictability limit established by Lorenz (1979), seasonal forecasts operate within a probabilistic forecasting framework. Probabilistic forecasts provide a range of possible outcomes and the likelihood of each outcome, rather than a single deterministic prediction. This is particularly important in climate forecasting, where the inherent uncertainty and complexity of atmospheric systems make it impossible to predict exact outcomes. This approach enables a more comprehensive understanding of potential future climate patterns, which is particularly useful for the design of sector-specific climate services that focus on time scales of one to six months (Crochemore et al. 2017), agriculture (Vajda and Hyvärinen 2020), energy (Goodess et al. 2022; Lledó et al. 2019) food (Eccel et al. 2016) infrastructure, water (Arnone et al. 2020a, b; Marcos et al. 2017), tourism, finance and insurance are some of the sectors where seasonal forecasts are commonly used for strategic and management decisions. The European Commission has made considerable efforts to promote research in the climate services field, funding several research projects, and creating specialised agencies and initiatives such as the Copernicus Climate Change Service (C3S), which offers open and free climate data for both research and business purposes.

The accuracy of seasonal forecasts depends on several factors, including variables, location, lead time, and season considered (An-Vo et al. 2021; Manzanas et al. 2022). Several metrics are used to measure the skill of seasonal forecasts, including Mean Bias, Mean Absolute Error (MAE), Anomaly Correlation Coefficient (ACC), Brier Skill Score (BSS), Ranked Probability Score (RPS), and its continuous version (CRPS). A description of the mathematical aspects of these metrics can be found in Wilks (2011) and Crespi et al. (2021). The seasonal forecasts must be systematically compared with a reference (reanalysis or observations) to assess their overall quality. In this paper, the ECMWF ERA5 reanalysis (Hersbach et al. 2020a) is used as a reference dataset.

In analysing the performance of seasonal forecasts, it is observed that temperature and pressure predictions generally yield higher skill scores compared to precipitation and wind (Landman and Beraki 2012; Mishra 2013). This discrepancy poses challenges in the reliability and application of these forecasts in climate services. In Southern Africa, the seasonal predictions have a higher skill during the austral summer, mainly due to the high predictability of the ENSO and its teleconnection to Southern Africa (Cook 2001). A negative anomaly in precipitation in Southern Africa is usually associated with El Niño events, while positive anomalies characterise East Africa. Conversely, during La Niña events, negative precipitation anomalies are observed in Southern Africa and positive anomalies in East Africa in summer (Indeje et al. 2000). Precipitation skills in Southern Africa are high during El Niño and La Niña but significantly decrease in neutral conditions, as observed by Landman et al. (2012). During the other seasons, autumn, winter and spring, the seasonal forecasts skills are significantly lower probably due to the weakness of the ENSO signal in those seasons. Gillett et al. (2006) also emphasised the role of the Southern Annular Mode (SAM) in the intra-seasonal variability of the precipitation: positive SAM implies positive precipitation anomalies in summer. Seasonal rainfall anomalies in Southern Africa show a low skill, sug-

gesting a need to understand why this inability of the SF is particularly pronounced in that region and whether it is possible to improve the quality of the forecast.

An open question in southern African climate science is whether the relatively low skill in predicting seasonal precipitation anomalies in winter and the transition seasons can be improved. Such improvements may result from model development, including improved initialisation and assimilation systems that better incorporate information about the ocean state, or long and planetary waves, which can translate to forecast skill at seasonal time scales. It is equally important to explore whether there are forms of external forcing that are not adequately accounted for in climate models and which, if included, can significantly improve predictive skill. Antarctic stratospheric ozone is a primary example in this regard. The importance of its concentrations for climate variability in the Southern Hemisphere troposphere is a relevant recent discovery (Thompson et al. 2011), and its impact on the interannual variability in southern Africa is still largely unexplored (Engelbrecht et al. 2015).

The ability of climate models to correctly predict the intensity of baroclinic instability is a very important prerequisite, as this phenomenon is a significant component of the climate system, associated with the meridional transport of a large amount of energy and momentum. Moreover, baroclinic instability can be linked to precipitation activity and its intensity. Consequently, evaluating the ability of seasonal forecasting to correctly predict baroclinic activity can contribute to understanding the ability of precipitation forecasting. These two physical phenomena are not directly related, but the energy associated with baroclinic instabilities can easily be associated with the development of mid-latitude fronts. Baroclinic instability, a key factor in the development of mid-latitude weather systems, was found to be closely linked to precipitation in several studies. Lambaerts et al. (2012) discussed the influence of water vapour condensation and latent heat release on the development of baroclinic instability, with the former finding that condensation significantly increases the growth rate of baroclinic instability and the latter assessing the role of hydrodynamic instability in the formation of precipitation in a cold-core low. Both Matsumoto et al. (1923) and Sáenz et al., (2001) found a correlation between baroclinic instability and precipitation. The former found that the interannual variability of winter precipitation in the northern Iberian Peninsula can be explained by baroclinic instability, and the latter found that the pre-summer rainy season in Japan is influenced by the vertical motions of baroclinic unstable waves. Recently, Yang and Li (2023) further investigated this relationship and proposed a theory of moist baroclinic instability to explain the development of synoptic disturbances along the subtropical Mei-Yu front.

In this paper, we examine the atmospheric dynamics that affect seasonal precipitation forecasts, with a particular focus on describing baroclinic instability in the Southern Hemisphere. We assume that the uncertainties in precipitation forecasting, and the relatively low accuracy of these predictions can be attributed not only to the inherent complexities in modelling the water cycle, but also to the suboptimal description of baroclinic instability and high-frequency dynamical components in the forecast models.

This research uses a space-time spectral analysis to quantify the energy content of atmospheric phenomena, by computing the Hayashi spectra of the 500-hPa geopotential height field (Hayashi 1971). The subsequent studies of Pratt (1976) and Fraedrich et al., (1978) reinterpreted the method for calculating the power spectra of space-time series. The analyses of Dell'Aquila et al., (2007a) and (2005) which we used as a starting point, are partly based on these studies. In particular, the methodology adopted in this study proves useful to

assess the performance of climate models in describing mid-latitude winter variability (Di Biagio et al. 2014; Lucarini et al. 2007). In addition, following the procedure described by Dell'Aquila et al., (2007a), we assess the Baroclinic Amplitude Index (BAI), an indicator that quantifies the intensity of baroclinic activity.

Dell'Aquila et al. (2007a) show, atmospheric planetary waves, especially in the Southern Hemisphere (SH), play a crucial role in shaping the Earth's climate system. Unlike the Northern Hemisphere, the SH lacks a pattern of mountain chains that could lock the phase of planetary-scale waves. As a result, the atmospheric variability is predominantly driven by eastward-propagating wave trains with both high and low frequencies. High frequencies, typically below 10 days, are dominated by the rise and decay of baroclinic disturbances, which effectively convert available potential energy into kinetic energy. Remarkably, baroclinic activity is more intense in the Southern Hemisphere than in the Northern Hemisphere, peaking around 50°S. We also extend this approach to seasonal forecasts to verify if we can obtain comparable results.

In a recent study by Zhang et al. (2021), the predictability of baroclinic wave activity has been investigated. The research highlights the significant spatio-temporal variability of these events and their interaction with other critical atmospheric phenomena, such as tropical cyclones. This interaction plays a pivotal role in the formation, trajectory, and intensity of these cyclones, highlighting the intricate dynamics of the atmosphere. Building on this knowledge, our study aims to assess the ability of seasonal forecasts to accurately describe these atmospheric patterns, as they have a significant impact on shaping atmospheric anomalies on time scales of a few days to several weeks, thus underpinning the accuracy and reliability of climate forecasts.

Weisheimer et al. (2020) conducted a thorough analysis of the ability of seasonal forecasts to accurately represent atmospheric dynamics and instabilities. This study pays particular attention to the performance of hindcasts in capturing mid-tropospheric flow, especially in relation to the North Atlantic Oscillation (NAO) and eddy-driven jet streams over the North Atlantic. Focusing on the predictability of baroclinic wave activities and their impacts on weather patterns, our study contributes to a more comprehensive understanding of global climate dynamics and seasonal forecasting uncertainties.

The paper is structured as follows: in Sect. 2 we describe the methods, including the Hayashi spectral technique and the computation of the Baroclinic Amplitude Index (BAI). In Sect. 3 we provide a description of the data and the study area. In Sect. 4 we present our analysis of the 500 hPa geopotential height field power content in these datasets, emphasising the role of baroclinic activity in the Southern Hemisphere. Additionally, we discuss the implications of our findings for improving seasonal forecast skills, particularly in terms of precipitation prediction in Southern Africa Finally, we conclude with a perspective on future research directions.

2 Methodology

In this study, we adopt the same approach as in Dell'Aquila et al. (2005) analysing the ability of seasonal forecasts to describe energy associated with mid-latitude variability in the atmosphere. To this end, we apply spectral analysis to study winter atmospheric variability across mid-latitudes of the Southern Hemisphere from 1993 to 2020, considering both the

hindcast and the forecast available to cover a larger time interval. Following the conclusion of the hindcast period and extending up to 2020, we chose an equal number of ensemble members from each originating centre randomly, mirroring the configuration employed during the hindcast period. We estimate the power content of the atmospheric phenomena typical of mid-latitudes, with a specific emphasis on baroclinic perturbations. We used the Hayashi technique, referring to Hayashi (1971) and Pratt (1976), to create the power spectra and distinguish the standing and travelling wave patterns. The spatio-temporal Fourier decomposition was introduced by Hayashi (1979) and (1971) to describe the variability of the geopotential height field in terms of periods and zonal wavenumbers. This technique enables creating power spectra of space-time series as a function of the frequencies ω and the wavenumbers k. The Hayashi method states that for a periodic series in space x and infinitely extended in time t, the power spectra can be divided into standing and travelling components. The total signal is the sum of these two components. Standing waves typically form due to the interference of two waves travelling in opposite directions (Georgi and French 1993). These waves are often associated with geographical features such as mountains that disrupt the wind flow, causing it to form a wave pattern. On the other hand, travelling waves are generated by instability in the atmospheric flow, often associated with variations in temperature and pressure. These waves propagate from one location to another, carrying energy and momentum with them. The decomposition of the original signal into its standing and travelling parts is based on the physical interpretation of these waves: travelling and standing waves are generated by different mechanisms and therefore attributable to different physical phenomena. Therefore, decomposing the signal enables to separately analyse the effects of these different phenomena. In our study, we chose the months June, July, and August (JJA) to analyse the Southern Hemisphere winter atmospheric variability. The three months have lead times equal to 1, 2, and 3 respectively, since we consider May as the forecast starting month. By dropping the first month of the forecast, we ensure that all ensemble members have lost track of their initial conditions and can be considered as statistically independent realisations of the atmospheric dynamics under the same driving conditions concerning the slow components of the climate systems (i.e. state of the ocean, land cover, ice cover). In particular, by dropping the first month of the forecast, the statistical independence is ensured both for the forecasts initialised in burst mode, i.e. all members start at the same time with perturbation designed to maximise the growth rate of initial anomalies (Molteni et al. 1996), and for the forecasts initialised in lagged mode, i.e. ensemble members are started on different dates to improve the skill of the forecast at subseasonal time scale (Chen et al. 2013).

To capture most of the baroclinic activity and low-frequency planetary waves, we chose the latitude range from 30°S to 75°S for both the reanalysis and seasonal forecasts datasets (Dell'Aquila et al. 2007a) and we performed a weighted average of the geopotential field within this latitudinal belt, obtaining a one-dimensional longitudinal field representative of the atmospheric variability at mid-latitudes. Consequently, the geopotential height field, originally varying both zonally and meridionally, exhibits spatial dependence only on longitude after averaging over the latitudinal direction. Afterward, we employed the Fourier space-time decomposition, specifically the Fast Fourier Transform (FFT) method, to obtain a geopotential height field in the domain of frequencies and wavenumbers, instead of time and longitude. Within this domain, we selectively filtered out frequencies corresponding to periods exceeding 10 days and set these values to zero. This high-pass filter enables to

isolate only the modes with a period of less than 10 days (Dell'Aquila et al. 2007b) and is a fundamental step for the final stage of our analysis, which entails the computation of the Baroclinic Amplitude Index (BAI). The BAI is useful for measuring baroclinic intensity and understanding how much energy is being released from the atmosphere in the form of rain and heat fluxes on Earth: the higher the index, the stronger the baroclinic activity.

The Baroclinic Amplitude Index is derived from the integral of the Fourier coefficients confined to zonal wavenumbers between 4 and 7. By focusing on this particular wavenumber range, the aim is to capture those components of atmospheric variability that are most affected by baroclinic energy conversion processes. However, as highlighted by Stoll et al. (2023), the same wavenumber can correspond to different processes at varying scales, particularly at higher latitudes. Stoll et al. (2023) propose an alternative approach, differentiating between synoptic and planetary waves based on wavelength rather than wavenumber. This method accounts for the latitude-independent nature of baroclinically induced transport anomalies, emphasising the physical distinction between these scales across different latitudes. Our selection of wavenumbers 4 to 7 in the BAI aims to capture baroclinic activity within the latitudinal belt of 35°S to 75°S. At higher latitudes, the deformation of the length scale becomes significant due to the Rossby deformation radius decreasing with latitude. This implies that the same wavenumber may represent different physical scales depending on the latitude, making the interpretation of associated phenomena challenging.

Our analysis takes into account that wavelengths larger than 8000 km are classified as planetary waves, while those around 5000 km or smaller are predominantly transient and baroclinic, aligning with the findings of Stoll et al. (2023). Specifically, our methodology acknowledges that while stationary waves dominate the larger wavelengths (with a peak for k=3, as shown in Fig. 1.b), the majority of baroclinic energy is found within higher wavenumbers (as shown in Fig. 1.c), consistent with the transient nature of baroclinic eddies. By distinguishing between these scales, our approach ensures that the contributions of both transient and stationary components are appropriately considered, thereby providing a comprehensive understanding of atmospheric variability and the change in spatial scale of transient eddies at higher latitudes.

The BAI is then calculated with the following formula:

$$Z_{4-7}(t) = \left(\sum_{k=4}^{7} 2|Z_k|^2 \right)^{\frac{1}{2}}$$

where Z_k are the Fourier coefficients of the zonal wavenumbers from 4 to 7.

2.1 Data

The analysis was applied to three seasonal forecast datasets, including the ECMWF Seasonal Forecast System 5 (SEAS5, 25 ensemble members), the Météo-France System 7 (25 ensemble members) and the DWD GCFS2.1 (30 ensemble members), accessible via the Copernicus Climate Data Store (CDS) ("Climate Data Store"). Seasonal forecasts consist of ensemble predictions, where each member of the ensemble represents an independent realisation of the forecast. Details regarding each model, such as ensemble size and horizontal resolution, can be found in Table 1. Forecasts made with SEAS5 and GCFS2.1 are initialised in burst mode, and by dropping the first month in the forecast we ensure statistical

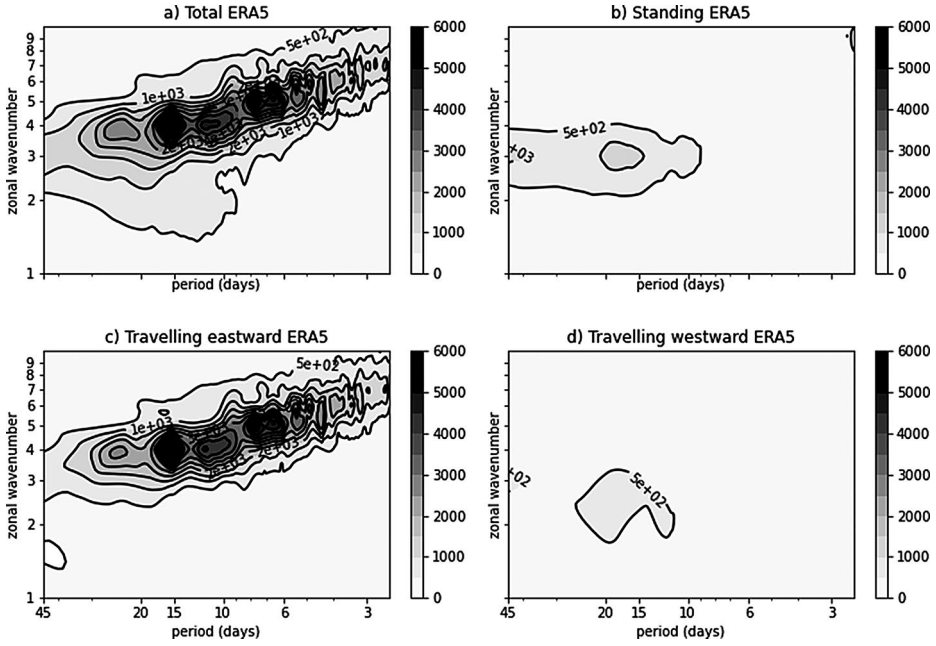

Fig. 1 Hayashi spectra for 500-hPa geopotential height from ERA5 averaged over the 28 winters (1993–2020) in the Southern Hemisphere (30–75°S). The figure is divided into four panels, each describing the geopotential height in terms of period (x axis) and zonal wavenumber (y axis): (**a**) total Hayashi spectra, given by the sum of travelling and standing waves. (**b**) standing wave component of the spectra, (**c**) eastward-travelling wave component of the spectra (**d**) westward-travelling wave component of the spectra

Table 1 List of models used with the number of the ensemble, the resolution, the hindcast period and the references. The horizontal resolution is approximate and refers to the native resolution of the forecasting systems

Forecasting system name	Forecasting centre	Hindcast ensemble size	Hindcast period	Horizontal resolution	Reference
SEAS5	ECMWF	25	1981–2016	36 km x 36 km	(Johnson et al. 2019)
System 7	Météo France	25	1993–2018	0.5° x 0.5°	(Voldoire et al. 2019)
GCFS2.1	DWD	30	1993–2019	100 km x 100 km	(Stevens et al. 2013)

independence of the ensemble members. For System 7, forecasts are normally initialised in lagged mode. However, the model simulations are initialised before the nominal starting date on which the forecast and corresponding hindcasts are published. Statistical independence is therefore also ensured for System 7. After the end of the hindcast period, until 2020, we have randomly selected for each source centre the same number of ensemble members as in the hindcast period, i.e. 25 members out of the 50 or 51 members available for the forecast period. Note that for the SEAS5 hindcast data are available from 1981 onwards. For

our analysis, however, we only consider data covering the common time frame from 1993 onwards. The horizontal resolution given in Table 1 refers to the native configuration of the atmospheric components of the forecast systems. For the analysis presented in this paper, however, we use data with a uniform resolution of 1°x1°, as provided by the CDS.

The reference dataset consists of the geopotential height fields of 500 hPa belonging to the ERA5 reanalysis (Hersbach et al. 2020b). Although ensemble members are available for ERA5 as a by-product of the data assimilation system, we use the single high-resolution realisation provided on CDS as the final reanalysis product. ERA5 is the fifth-generation global reanalysis of the ECMWF and spans from 1950 to the present with an hourly temporal resolution, on a regular $0.25° \times 0.25°$ grid. To maintain consistency with the seasonal forecasts datasets, we reduced the spatial resolution of ERA5 from 0.25° to 1° before performing the calculations described in Sect. 3. This was achieved through a nearest-neighbour interpolation applied to the time-longitude-dependent geopotential height field.

3 Results

3.1 Hayashi spectra of ERA5 reanalysis

Figure 1 shows the Hayashi spectra of the 500-hPa geopotential height averaged over the 28 winters from 1993–2020, calculated from the ERA5 reanalysis dataset. In particular, the four components of the spectra are displayed: total, stationary, travelling eastward and travelling westward.

The spectra express the power density of the wave field in terms of frequency and zonal wavenumber. When looking at the total power spectrum (a), the darker colours show that a large fraction of the total power is concentrated in periods between 4 and 16 days and in wavenumbers between 3 and 7. In this region we can identify the baroclinic disturbances, travelling waves with a period in the order of 2–7 days, wavenumbers around 4–7 m^{-1} and a spatial extent of several thousand kilometres. This domain is related to the eastward propagating waves (c) and includes the synoptic phenomena associated with the release of available energy driven by conventional baroclinic conversion (Blackmon 1976). These phenomena contribute to the energy transfer in the Southern Hemisphere at mid-latitudes, leading to atmospheric stability or instability. Although the overall variability is mainly explained by the eastward propagation component, we can see that it also extends to planetary scales, with k = 3–4 and a period of about 16 days.

Standing waves (b) are characterised by low frequencies (long periods) and low wavenumbers, and in the Northern Hemisphere they are mainly driven by the Rocky Mountains (Holton et al., 2012). In the Southern Hemisphere, they exhibit a peak in wavenumber around 3 m^{-1}, which could be associated with blocking episodes due to the presence of the Andes. However, they play a smaller role, as the Andes do not appear to contribute significantly to the amplification of planetary waves (de Adana et al., 2005).

3.2 Hayashi spectra of SEAS5 seasonal forecast

Figure 2 illustrates the Hayashi spectra average over the members of the SEAS5 ensemble. The plots were generated by calculating the Hayashi spectra for each member and then by

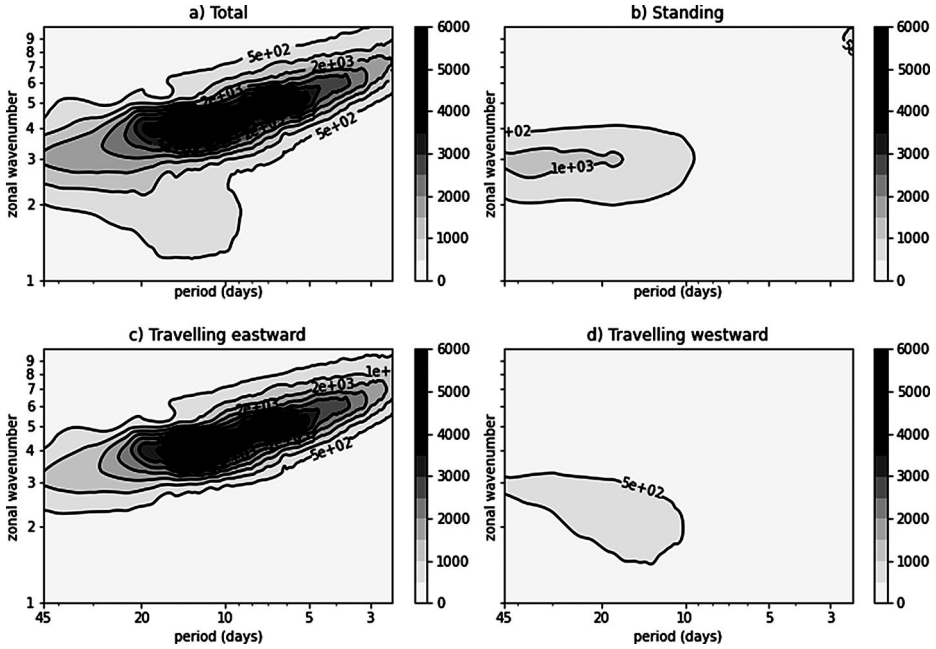

Fig. 2 Hayashi spectra for 500-hPa geopotential height from SEAS5 averaged over the 28 winters (1993–2020) in the Southern Hemisphere (30–75°S). The figure is divided into four panels, each describing the geopotential height in terms of period (x axis) and zonal wavenumber (y axis): (**a**) total Hayashi spectra, given by the sum of travelling and standing waves. (**b**) standing wave component of the spectra, (**c**) eastward-travelling wave component of the spectra (**d**) westward-travelling wave component of the spectra

computing the average over the entire ensemble. This process naturally smooths out the peaks, making them less pronounced compared to analysing each element separately. However, we found that calculating a representative average spectrum of the entire ensemble is more informative than analysing the individual members separately, as these were generated with random perturbations to the initial conditions. Nevertheless, Fig. 2 indicates that, similar to the reanalysis, also for the seasonal forecasts the overall variability of the power spectrum of the 500-hPa geopotential height is mainly explained by the eastward propagating component, extending to the planetary scales (k = 3–4 and period around 15 days or more).

Figure 3 shows the standard deviation of the SEAS5 ensemble. Using this metric, we can understand where the greatest variability exists among all the spectra of the ensemble members.

The analysis of standard deviation across the spectra of seasonal forecasts highlighted distinct patterns. In particular, for wavenumber k = 4, the variability of the signal spans frequencies associated with periods ranging from 18 to 8 days. There is a pronounced peak within the 18 to 11-day range, accompanied by weaker maxima between 10 and 8 days. For wavenumber k = 5, we observe heightened variability for periods between 10 and 5 days, with the most pronounced peaks occurring between 8 and 5 days. This pattern indicates substantial differences in the behaviour of the various ensemble models compared to what is observed in the ERA5 reanalysis data.

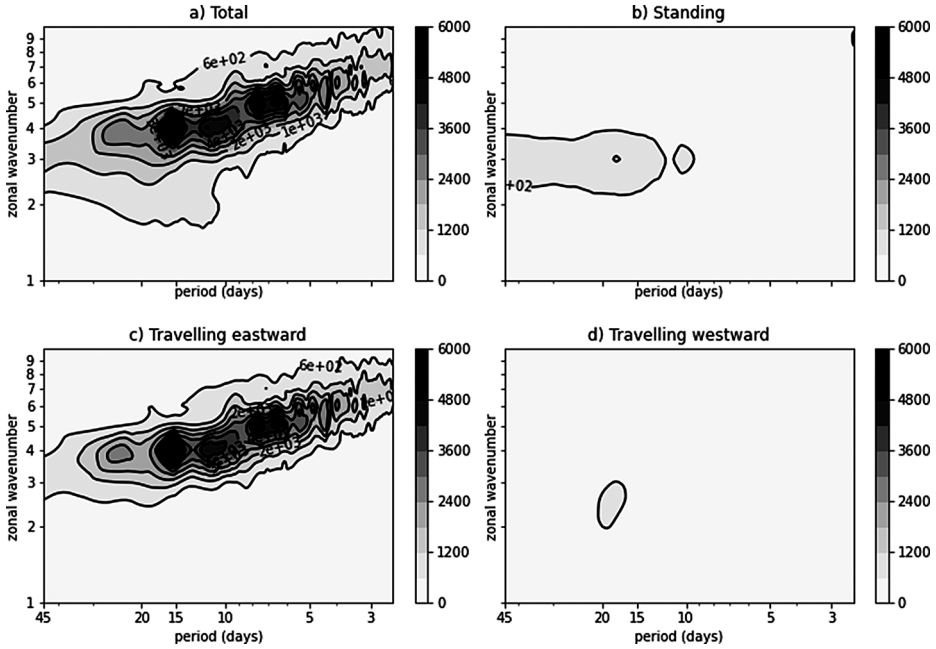

Fig. 3 Standard deviation of the SEAS5 ensemble Hayashi spectra for the 500-hPa geopotential height in terms of period and zonal wavenumber, averaged over the 24 winters. The four panels refer to: (**a**) total Hayashi spectra, (**b**) standing wave component of the spectra, (**c**) eastward-travelling wave component of the spectra (**d**) westward-travelling wave component of the spectra

This contrast is also visible when comparing Figs. 1 and 2. For wavenumber 4 and 5, the peaks in ERA5 are centered around 15 and 7 days, respectively, with a gradual decline in the energy surrounding these values (Fig. 1, panels a and c). Conversely, the ensemble members of the seasonal forecasts (Fig. 2, panels a and c) display greater variability in period space, which suggests a challenge in the ability of seasonal forecast ensembles to accurately capture the dynamical energy distribution of the observed field. This discrepancy indicates potential limitations in the representation of atmospheric dynamics by current ensemble models, highlighting an area for further investigation and model refinement.

3.3 Difference between seasonal forecasts and ERA5

The comparison between ERA5 and the seasonal forecasting systems covers two different aspects. We first consider a comparison between the average spectrum based on ERA5 and the corresponding ensemble mean derived from the forecasting systems, to assess the systematic biases. Afterwards, we focus on the spread of the ensemble members by focusing on the spectral components associated to the BAI as defined in Sect. 3.

Figure 4, 5 and 6 show the mean differences between the Hayashi spectra derived from SEAS5, System 7 and GCFS2.1, respectively, and those computed using ERA5. For each of these three seasonal forecasts, we first computed an ensemble mean of the spectra, and then subtracted the reanalysis spectra.

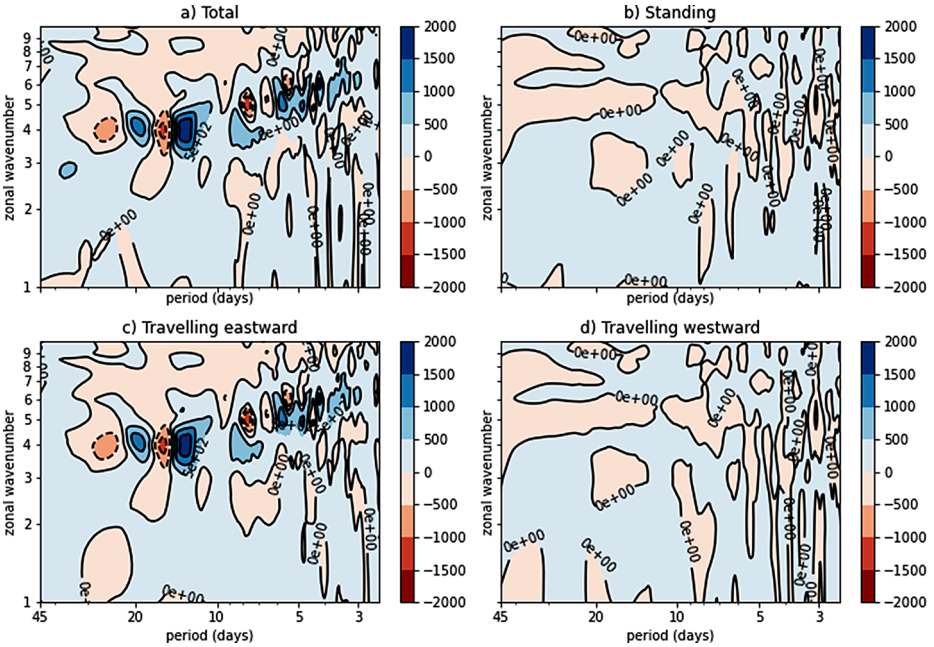

Fig. 4 Difference between SEAS5 and ERA5 Hayashi spectra for 500-hPa geopotential height averaged over the 28 winters and over the ensemble. The four panels refer to: (**a**) total Hayashi spectra, (**b**) standing wave component of the spectra, (**c**) eastward-travelling wave component of the spectra (**d**) westward-travelling wave component of the spectra

While minimal differences are observed for standing and westward waves in all three cases (Figs. 4b-d, 5b-d, 6b-d), larger discrepancies arise for eastward waves (Figs. 4c, 5c, 6c). For SEAS5 and GCFS2.1, a distinct peak of positive bias (in blue) emerges for periods around 12 days and wavenumber 4, indicating that in this spectral region, the variability detected by the seasonal forecasts is much larger compared to ERA5. This overestimation is less pronounced for System 7 (Fig. 6a-c), where the blue peak around wavenumber 4 and 12–15 days is partially offset by the negative peaks (light red) around 15–17 days. Moreover, there is greater variability between 4 and 7 days, as can be inferred from the alternating red and blue peaks in this region.

For more insight into the intensity and variability of the baroclinic activity, we analysed the Baroclinic Amplitude Index (BAI), described in Sect. 3. The BAI is calculated for each day of the time series. Through this analysis it is possible, on the one hand, to observe the change in the index over the years and, on the other hand, to understand whether seasonal forecasts can calculate it correctly in comparison with the reanalysis. The objective of this analysis is twofold. On one hand, the focus is on interannual variability to understand how the seasonal forecasts compare with observations. On the other hand, the spread of the ensemble members can be compared both with the interannual variability and with the model bias to understand whether any useful signal can be extracted from the forecasts.

To illustrate the distribution of BAI within the ensemble, we use box plots (Figs. 7, 8 and 9), which represent the distribution of BAI values for each year among the ensemble members, indicating the variability within the ensemble. The centre line in the box repre-

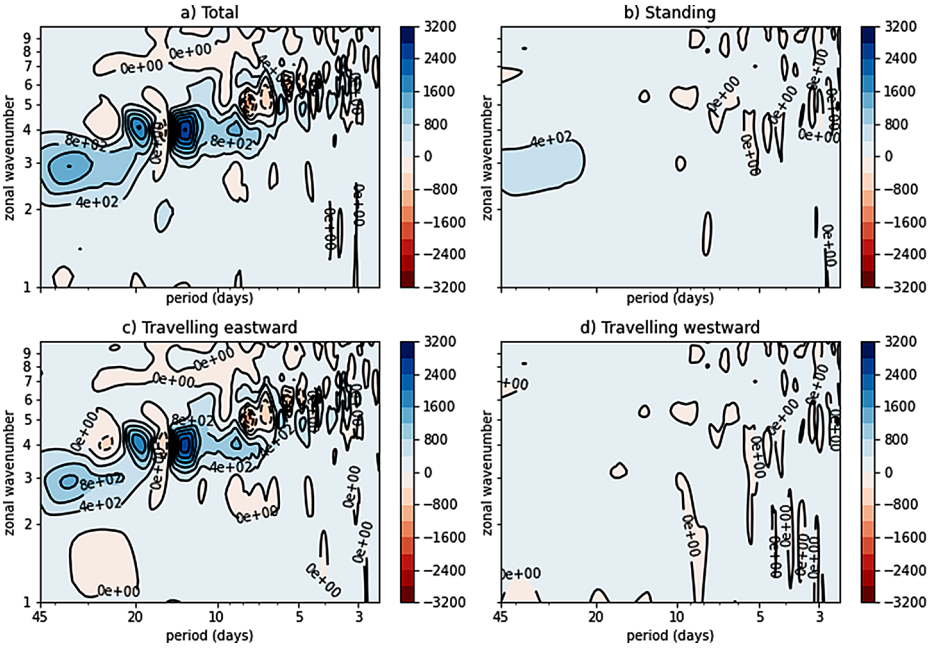

Fig. 5 Difference between GCFS2.1 (DWD) and ERA5 Hayashi spectra for 500-hPa geopotential height averaged over the 28 winters and over the ensemble. The four panels refer to: (**a**) total Hayashi spectra, (**b**) standing wave component of the spectra, (**c**) eastward-travelling wave component of the spectra (**d**) westward-travelling wave component of the spectra

sents the median of the data and the mean is shown as a green triangle. The BAI values are computed considering zonal wavenumbers between 4 and 7 and the latitudinal belt between 30 and 75°S.

Figures 7, 8 and 9 show that the average annual BAI, calculated using reanalysis data and represented by the blue line, exhibits significant interannual variability. Zhang et al. (2021) noted how a long-standing obstacle to exploring the predictability of the baroclinic wave amplitude is the weak responses of the extratropical atmosphere to climate forcings, such as sea surface temperature (SST) forcings. Indeed, the seasonal forecasts reported in Figs. 7, 8 and 9, show limited variability in the ensemble mean and particularly weak performances in capturing extreme fluctuations. In general, the BAI is overestimated by the seasonal forecasts, in particular for the DWD forecast model (Fig. 8), consistently with the analysis presented in Fig. 6. In this respect, the seasonal forecasts of Météo France have a relatively better alignment with the reanalysis data, showing a less pronounced overestimation.

For a quantitative comparison between the variability of the Baroclinic Amplitude Index observed in the ERA5 reanalysis and the corresponding variability described by the seasonal forecasts, some statistics of the signals described in Figs. 7, 8 and 9 are reported in Table 2. The comparison of the mean BAI reflects the systematic biases already discussed above, with GCFS2.1 showing the largest bias among the models considered for the analysis. The variance of the ensemble mean of the seasonal forecasts (the green triangles in Figs. 7, 8 and 9) quantifies the relatively low variability of the forecasts compared to the ERA5 reanalysis. Furthermore, the mean ensemble variance, which is obtained by comput-

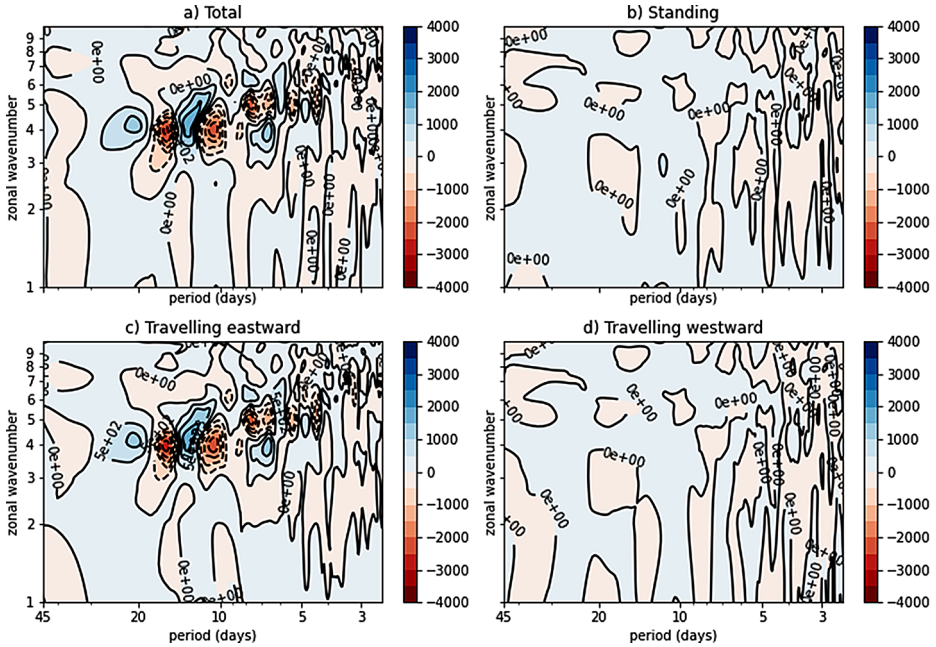

Fig. 6 Difference between System 7 (Météo France) and ERA5 Hayashi spectra for 500-hPa geopotential height averaged over the 28 winters and over the ensemble. The four panels refer to: (**a**) total Hayashi spectra, (**b**) standing wave component of the spectra, (**c**) eastward-travelling wave component of the spectra (**d**) westward-travelling wave component of the spectra

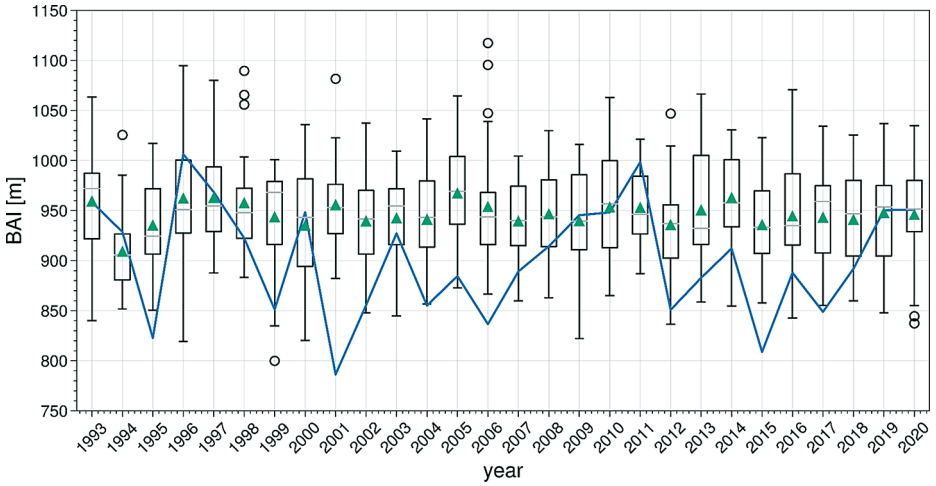

Fig. 7 Yearly averaged BAI of the ensemble members for SEAS5 (boxplot) and yearly averaged BAI for ERA5 (blue line). The integration is computed between k=4 and k=7

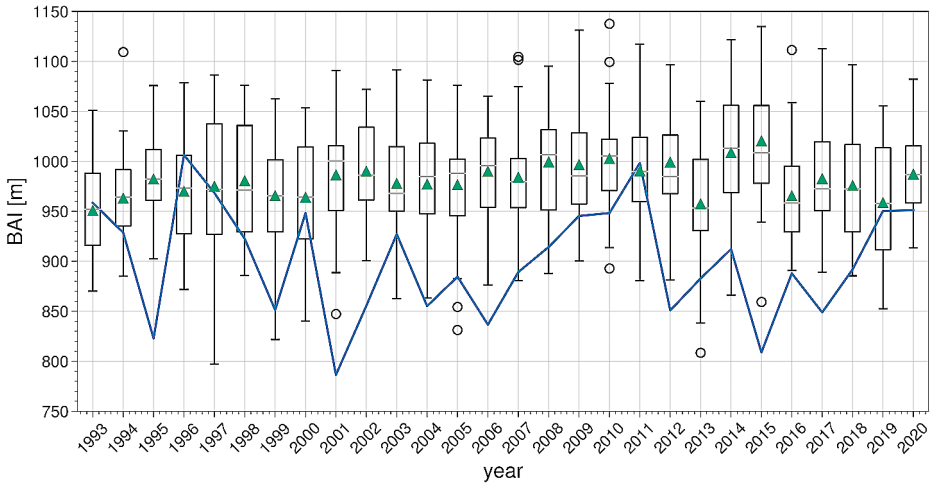

Fig. 8 Yearly averaged BAI of the ensemble members for DWD (boxplot) and yearly averaged BAI for ERA5 (blue line). The integration is computed between k = 4 and k = 7

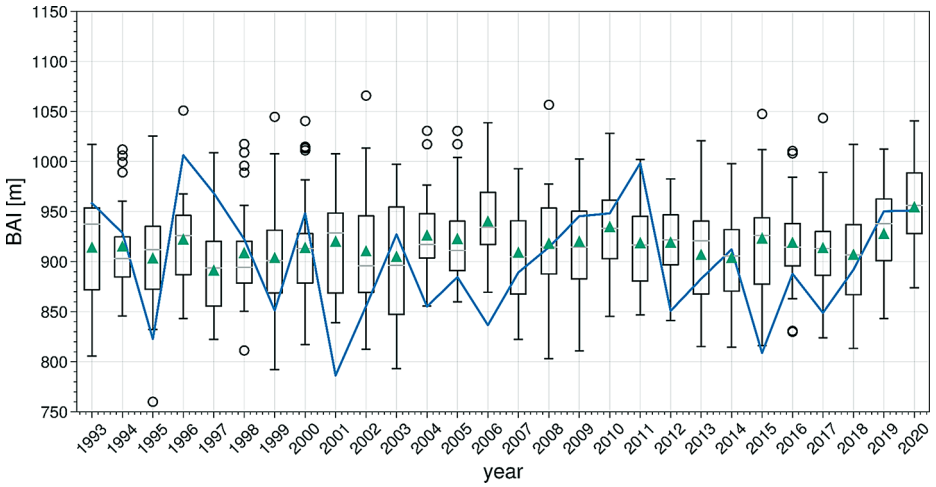

Fig. 9 Yearly averaged BAI of the ensemble members for Météo France (boxplot) and yearly averaged BAI for ERA5 (blue line). The integration is computed between k = 4 and k = 7

Table 2 Analysis of the BAI in the reanalysis and seasonal forecasts. The "Variance" column is obtained by computing the variance of the ensemble mean of the seasonal forecasts. The "Mean ensemble variance" column is obtained by computing the variance among the ensemble members for each year and then averaging over all years

Model	Mean [m]	Variance [m^2]	Mean ensemble variance [m^2]
ERA5	901	3214	-
SEAS5	946	143	2508
GCFS2.1	981	271	3096
System 7	917	161	2459

ing the variance among the ensemble members for each year and then averaging over all years, is about 10 to almost 20 times larger than the variance of the ensemble mean. This generally corresponds to a relatively low signal-to-noise ratio, making it difficult to extract useful information from this limited time series. On the other hand, the ensemble mean variance of the forecast systems reported in Table 2 is comparable to the variance of the BAI observed in ERA5. This implies that, if the systematic bias were removed, most of the BAI values computed with ERA5 would be within one standard deviation of the ensemble mean of the corresponding forecast. This effect is more easily seen in the case of System 7 (Fig. 9), which is characterised by a relatively smaller bias.

Overall, this analysis shows, consistently with the findings of Zhang et al. (2021), that it is currently impractical to extract from seasonal forecasts some useful information about the expected intensity of the baroclinic activity in the southern hemisphere.

4 Conclusions

In this study, we performed a statistical analysis of baroclinic instability in the Southern Hemisphere. Our analysis, based on the spectral decomposition of the 500-hPa geopotential height field, provides useful insights into the behaviour of seasonal forecast models in describing the mechanisms of mid-latitude atmospheric variability, as compared to the ERA5 reanalysis.

The results emphasise the expected predominant influence of the eastward propagation component in explaining winter variability in the Southern Hemisphere. In particular, the analysis reveals a series of peaks and structures that can be attributed to the phenomenology of eastward-propagating baroclinic waves.

The focus of our study on the Baroclinic Amplitude Index (BAI) provides valuable insights into the intensity of baroclinic activity. However, the seasonal forecasts struggle to capture the interannual variability of baroclinic activity as effectively as the reanalysis data. This is illustrated by the relatively constant winter BAI in the seasonal forecasts, in contrast to the larger fluctuations observed in the reanalysis. In addition, the seasonal forecasts tend to overestimate the BAI, a factor that could contribute to reducing the skill of the forecasts in predicting the associated events that may be of immediate interest for sectoral applications (e.g. accumulated precipitation, frequency of extreme temperatures).

The comparison of the ERA5 reanalysis data with SEAS5, GCFS2.1 and System 7 seasonal forecasts revealed remarkable differences in the representation of baroclinic instability. These differences were most pronounced for the eastward propagating components of the wave spectrum and suggest areas where the seasonal forecast models can be improved. In particular, we identified a specific problem in the distribution of energy both in space (for an 8-day period) and in time (for wavenumber 4). This indicates difficulties in accurately representing the structure of the baroclinic instability, particularly with respect to the spatial and temporal distribution of energy. These challenges may result from the limited ability of the models to capture the complex dynamics of baroclinic instability, including the interaction of different scales of motion and the influence of various physical processes.

Our results suggest that an improvement in the accuracy and reliability of seasonal forecasts entails a better representation of baroclinic waves. At the moment, it appears impractical to extract from seasonal forecasts some useful information about the expected intensity

of the baroclinic activity in the southern hemisphere. Similar to the results discussed in Di Biagio et al. (2014) and Lucarini et al. (2007), which focused on CMIP models, our research highlights that seasonal forecasts may still benefit significantly from improvements in the initialisation of the state of the ocean and the land surface, as well as from an increase in horizontal and especially vertical resolution, which are the key factors for an accurate description of the atmospheric waves dynamics.

The relationship between the accurate representation of a physical mechanism's statistics in a model and the resulting predictive ability is not straightforward. It is a common misconception that improving the accuracy with which a model represents the statistics of a physical process necessarily increases its predictive accuracy. In this study, we emphasise that rather the opposite is true: if a physical process is modelled inaccurately, the predictability of the model is likely to be impaired. This principle emphasises the need for a precise representation of physical mechanisms in forecasting models, as errors in their representation can significantly affect the overall predictive ability of the model.

Acknowledgements This research is funded by the EU H2020 FOCUS Africa Project GA869575. L.T., S.d.G., M.V. and M.P. thanks the FOCUS-AFRICA project team for their wider contributions to the research. M.P. thanks the European Union—FSE-REACT-EU, PON Research and Innovation 2014-2020 DM1062/2021 for the financial support.

Author contributions Conceptualization, M.P. A.d.A. and S.C.; Methodology, L.T., M.P., A.d.A. and S.C.; Software, A.d.A., L.T. and M.V.; validation L.T., A.d.A. and S.D.G., Formal analysis, A.d.A., L.T., M.P. and S.C.; Investigation, L.T., S.C. and M.P.; resources, M.V.; Data curation, L.T., M.V., S.C. and S.D.G.; Writing - Original draft preparation, L.T. and M.P.; Writing—Review and editing, L.T., A.d.A., M.P., S.D.G. and S.C.; Supervision, M.P, A.d.A. and S.C.; Project administration, L.T; Funding acquisition, M.P. All authors have read and agreed to the published version of the manuscript.

Funding This research is funded by the EU H2020 FOCUS Africa Project GA869575. M.P. thanks the European Union—FSE-REACT-EU, PON Research and Innovation 2014–2020 DM1062/2021 for the financial support.
Open access funding provided by Università degli Studi di Roma Tor Vergata within the CRUI-CARE Agreement.

Data availability Geopotential Height data from ERA5 and the three seasonal forecast models are available at https://cds.climate.copernicus.eu.

Declarations

Competing interests The authors declare no competing interests.

References

An-Vo DA, Radanielson AM, Mushtaq S, Reardon-Smith K, Hewitt C (2021) A framework for assessing the value of seasonal climate forecasting in key agricultural decisions. Clim Serv 22:100234. https://doi.org/10.1016/J.CLISER.2021.100234

Arnone E, Cucchi M, Dal Gesso S, Petitta M, Calmanti S (2020a) Droughts prediction: a methodology based on climate seasonal forecasts. Water Resour Manage 34:4313–4328. https://doi.org/10.1007/s11269-020-02623-3

Arnone E, Stavridis GC, Ortolani L, Rammos A, Cucchi M, Gkiourou A, Gesso D, Petitta S, Psomas M, V (2020b) The drought-alert decision support system for water resources management. Desalin Water Treat 194:304–314

Blackmon ML (1976) A climatological spectral study of the 500 mb geopotential height of the Northern Hemisphere. J Atmos Sci 33:1607–1623. https://doi.org/10.1175/1520-0469(1976)033<1607:ACSSOT>2.0.CO;2

Chen M, Wang W, Kumar A (2013) Lagged ensembles, Forecast Configuration, and Seasonal predictions. Mon Weather Rev 141:3477–3497. https://doi.org/10.1175/MWR-D-12-00184.1

Climate Data Store [WWW Document] n.d. URL https://cds.climate.copernicus.eu/#!/home (accessed 5.31.24)

Cook KH (2001) A Southern Hemisphere Wave response to ENSO with Implications for Southern Africa Precipitation. J Atmos Sci 58:2146–2162. https://doi.org/10.1175/1520-0469(2001)058<2146:ASHWRT>2.0.CO;2

Crespi A, Petitta M, Marson P, Viel C, Grigis L (2021) Verification and bias adjustment of ecmwf seas5 seasonal forecasts over europe for climate service applications. Climate 9:181. https://doi.org/10.3390/CLI9120181/S1

Crochemore L, Ramos MH, Pappenberger F, Perrin C (2017) Seasonal streamflow forecasting by conditioning climatology with precipitation indices. Hydrol Earth Syst Sci. https://doi.org/10.5194/hess-21-1573-2017

de Adana FJ, Colucci SJ (2005) Ageostrophic relative vorticity forcing in the upper troposphere associated with the onset of blocking in the Southern Pacific [WWW Document]. Proceedings of 15th Conference on Atmospheric and Oceanic Fluid Dynamics. URL https://ams.confex.com/ams/Cambridge/techprogram/paper_89762.htm (accessed 6.2.24)

Dell'Aquila A, Lucarini V, Ruti PM, Calmanti S (2005) Hayashi spectra of the northern hemisphere midlatitude atmospheric variability in the NCEP-NCAR and ECMWF reanalyses. Clim Dyn. https://doi.org/10.1007/s00382-005-0048-x

Dell'Aquila A, Ruti PM, Calmanti S, Lucarini V (2007a) Southern Hemisphere midlatitude atmospheric variability of the NCEP-NCAR and ECMWF reanalyses. J Geophys Research: Atmos 112:8106. https://doi.org/10.1029/2006JD007376

Dell'Aquila A, Ruti PM, Sutera A (2007b) Effects of the baroclinic adjustment on the tropopause in the NCEP-NCAR reanalysis. Clim Dyn 28:325–332. https://doi.org/10.1007/S00382-006-0199-4

Di Biagio V, Calmanti S, Dell'aquila A, Ruti PM, Biagio V, Di M (2014) Northern Hemisphere winter midlatitude atmospheric variability in CMIP5 models. Geophys Res Lett 41, 1277–1282. https://doi.org/10.1002/2013GL058928

Eccel E, Zollo AL, Mercogliano P, Zorer R (2016) Simulations of quantitative shift in bio-climatic indices in the viticultural areas of Trentino (Italian Alps) by an open source R package. Comput Electron Agric 127:92–100. https://doi.org/10.1016/J.COMPAG.2016.05.019

Engelbrecht F, Adegoke J, Bopape MJ, Naidoo M, Garland R, Thatcher M, McGregor J, Katzfey J, Werner M, Ichoku C, Gatebe C (2015) Projections of rapidly rising surface temperatures over Africa under low mitigation. Environ Res Lett 10:085004. https://doi.org/10.1088/1748-9326/10/8/085004

Fraedrich Klaus B, Horst (1978) A wavenumber-frequency analysis of the 500 mb geopotential at 50°N [WWW Document]. Journal of the Atmospheric Science. URL (accessed 7.29.22).

Georgi H, French AP (1993) Phys Waves Phys Today 46:120–122. https://doi.org/10.1063/1.2809071

Gillett NP, Kell TD, Jones PD (2006) Regional climate impacts of the Southern Annular Mode. Geophys Res Lett 33:23704. https://doi.org/10.1029/2006GL027721

Goodess CM, Troccoli A, Vasilakos N, Dorling S, Steele E, Amies JD, Brown H, Chowienczyk K, Dyer E, Formenton M, Nicolosi AM, Calcagni E, Cavedon V, Perez VE, Geertsema G, Krikken F, Nielsen KL, Petitta M, Vidal J, De Ruiter M, Savage I, Upton J (2022) The Value-Add of Tailored Seasonal Forecast Information for Industry Decision Making. Climate 2022, Vol. 10, Page 152 10, 152. https://doi.org/10.3390/CLI10100152

Hayashi Y (1971) A generalized method of resolving disturbances into progressive and retrogressive waves by Space Fourier and Time cross-spectral analyses. J Meteorological Soc Japan Ser II 49:125–128. https://doi.org/10.2151/JMSJ1965.49.2_125

Hayashi Y (1979) A generalized method of resolving transient disturbances into standing and traveling waves by space-time spectral analysis. J Atmos Sci 36:1017–1029

Hersbach H, Bell B, Berrisford P, Hirahara S, Horányi A, Muñoz-Sabater J, Nicolas J, Peubey C, Radu R, Schepers D, Simmons A, Soci C, Abdalla S, Abellan X, Balsamo G, Bechtold P, Biavati G, Bidlot J, Bonavita M, De Chiara G, Dahlgren P, Dee D, Diamantakis M, Dragani R, Flemming J, Forbes R, Fuentes M, Geer A, Haimberger L, Healy S, Hogan RJ, Hólm E, Janisková M, Keeley S, Laloyaux P, Lopez P, Lupu C, Radnoti G, de Rosnay P, Rozum I, Vamborg F, Villaume S, Thépaut JN (2020a) The ERA5 global reanalysis. Q J R Meteorol Soc 146:1999–2049. https://doi.org/10.1002/QJ.3803

Hersbach H, Bell B, Berrisford P, Hirahara S, Horányi A, Muñoz-Sabater J, Nicolas J, Peubey C, Radu R, Schepers D, Simmons A, Soci C, Abdalla S, Abellan X, Balsamo G, Bechtold P, Biavati G, Bidlot J, Bonavita M, De Chiara G, Dahlgren P, Dee D, Diamantakis M, Dragani R, Flemming J, Forbes R, Fuentes M, Geer A, Haimberger L, Healy S, Hogan RJ, Hólm E, Janisková M, Keeley S, Laloyaux P, Lopez P, Lupu C, Radnoti G, de Rosnay P, Rozum I, Vamborg F, Villaume S, Thépaut JN (2020b) The ERA5 global reanalysis. Q J R Meteorol Soc 146:1999–2049. https://doi.org/10.1002/QJ.3803

Holton JR, Hakim GJ (2012) An introduction to dynamic meteorology. Introduction Dynamic Meteorology: Fifth Ed 9780123848666:1–532. https://doi.org/10.1016/C2009-0-63394-8

Indeje M, Semazzi FHM, Ogallo LJ (2000) ENSO signals in east African rainfall seasons. Int J Climatol 20:19–46

Johnson SJ, Stockdale TN, Ferranti L, Balmaseda MA, Molteni F, Magnusson L, Tietsche S, Decremer D, Weisheimer A, Balsamo G, Keeley SPE, Mogensen K, Zuo H, Monge-Sanz BM (2019) SEAS5: the new ECMWF seasonal forecast system. Geosci Model Dev 12:1087–1117. https://doi.org/10.5194/GMD-12-1087-2019

Lambaerts J, Lapeyre G, Zeitlin V (2012) Moist versus dry baroclinic instability in a simplified two-Layer Atmospheric Model with Condensation and Latent Heat Release. J Atmos Sci 69:1405–1426. https://doi.org/10.1175/JAS-D-11-0205.1

Landman WA, Beraki A (2012) Multi-model forecast skill for mid-summer rainfall over southern Africa. Int J Climatol 32:303–314. https://doi.org/10.1002/JOC.2273

Lledó L, Torralba V, Soret A, Ramon J, Doblas-Reyes FJ (2019) Seasonal forecasts of wind power generation. Renew Energy 143:91–100. https://doi.org/10.1016/J.RENENE.2019.04.135

Lorenz EN (1979) Forced and free variations of Weather and Climate. J Atmos Sci 36:1367–1376. https://doi.org/10.1175/1520-0469(1979)036<1367:FAFVOW>2.0.CO;2

Lucarini V, Calmanti S, Dell'Aquila A, Ruti PM, Speranza A (2007) Intercomparison of the northern hemisphere winter mid-latitude atmospheric variability of the IPCC models. Clim Dyn 28:829–848. https://doi.org/10.1007/S00382-006-0213-X

Manzanas R, Torralba V, Lledó L, Bretonnière PA (2022) On the reliability of global Seasonal forecasts: sensitivity to ensemble size, Hindcast Length and region definition. Geophys Res Lett 49:e2021GL094662. https://doi.org/10.1029/2021GL094662

Marcos R, Llasat MC, Quintana-Seguí P, Turco M (2017) Seasonal predictability of water resources in a Mediterranean freshwater reservoir and assessment of its utility for end-users. Sci Total Environ 575:681–691. https://doi.org/10.1016/J.SCITOTENV.2016.09.080

Matsumoto S, Itoo H, Arakawa A (1923) An Aerological Study on the Pre-summer Rainy season in Japan. J Meteorological Soc Japan Ser II 32:85–95. https://doi.org/10.2151/jmsj1923.32.4_85

Mishra V (2013) Food Security Implications of Climate Variability and Climate Change, Climate Vulnerability: Understanding and Addressing Threats to Essential Resources. Elsevier. https://doi.org/10.1016/B978-0-12-384703-4.00223-9

Molteni F, Buizza R, Palmer TN, Petroliagis T (1996) The ECMWF Ensemble Prediction System: methodology and validation. Q J R Meteorol Soc 122:73–119. https://doi.org/10.1002/QJ.49712252905

Pratt RW (1976) The interpretation of space-time spectral quantities. J Atmos Sci 33:1060–1066. https://doi.org/10.1175/1520-0469(1976)033<1060:TIOSTS>2.0.CO;2

Sáenz J, Zubillaga J, Rodríguez-Puebla C (2001) Baroclinic activity and interannual variability of Winter Precipitatio n in the Northern Iberian Peninsula. Detecting and modelling Regional Climate Change. Springer, Berlin Heidelberg, pp 405–416. https://doi.org/10.1007/978-3-662-04313-4_35

Stevens B, Giorgetta M, Esch M, Mauritsen T, Crueger T, Rast S, Salzmann M, Schmidt H, Bader J, Block K, Brokopf R, Fast I, Kinne S, Kornblueh L, Lohmann U, Pincus R, Reichler T, Roeckner E (2013) Atmospheric component of the MPI-M Earth System Model: ECHAM6. J Adv Model Earth Syst 5:146–172. https://doi.org/10.1002/JAME.20015

Stoll PJ, Graversen RG, Messori G (2023) The global atmospheric energy transport analysed by a wavelength-based scale separation. Weather Clim Dynamics 4:1–17. https://doi.org/10.5194/WCD-4-1-2023

Thompson DWJ, Solomon S, Kushner PJ, England MH, Grise KM, Karoly DJ (2011) Signatures of the Antarctic ozone hole in Southern Hemisphere surface climate change. Nat Geosci 4:741–749. https://doi.org/10.1038/NGEO1296

Vajda A, Hyvärinen O (2020) Development of seasonal climate outlooks for agriculture in Finland. Adv Sci Res 17:269–277. https://doi.org/10.5194/ASR-17-269-2020

Voldoire A, Saint-Martin D, Sénési S, Decharme B, Alias A, Chevallier M, Colin J, Guérémy JF, Michou M, Moine MP, Nabat P, Roehrig R, Salas y Mélia D, Séférian R, Valcke S, Beau I, Belamari S, Berthet S, Cassou C, Cattiaux J, Deshayes J, Douville H, Ethé C, Franchistéguy L, Geoffroy O, Lévy C, Madec G, Meurdesoif Y, Msadek R, Ribes A, Sanchez-Gomez E, Terray L, Waldman R (2019) Evaluation of CMIP6 DECK experiments with CNRM-CM6-1. J Adv Model Earth Syst 11:2177–2213. https://doi.org/10.1029/2019MS001683

Weisheimer A, Befort DJ, MacLeod D, Palmer T, O'Reilly C, Strømmen K (2020) Seasonal forecasts of the Twentieth Century. Bull Am Meteorol Soc 101:E1413–E1426. https://doi.org/10.1175/BAMS-D-19-0019.1

Wilks DS (2011) Statistical methods in the Atmospheric sciences. Int Geophys. https://doi.org/10.1016/B978-0-12-385022-5.00015-4

Yang G, Li T (2023) Moist baroclinic instability along the Subtropical Mei-Yu Front. J Clim 36:805–822. https://doi.org/10.1175/jcli-d-22-0140.1

Zhang G, Murakami H, Cooke WF, Wang Z, Jia L, Lu F, Yang X, Delworth TL, Wittenberg AT, Harrison MJ, Bushuk M, McHugh C, Johnson NC, Kapnick SB, Tseng KC, Zhang L (2021) Seasonal predictability of baroclinic wave activity. Npj Clim Atmospheric Sci 2021 4(1 4):1–11. https://doi.org/10.1038/s41612-021-00209-3

Authors and Affiliations

Laura Trentini[1] · Sandro Calmanti[2] · Alessandro Dell'Aquila[2] · Sara Dal Gesso[1] · Marco Venturini[1] · Marcello Petitta[1,3]

✉ Marcello Petitta
marcello.petitta@uniroma2.it

[1] Amigo s.r.l, Rome, Italy

[2] National Agency for New Technologies, Energy and Sustainable Economic Development, Rome, Italy

[3] University of Rome Tor Vergata, Rome, Italy